

# Tuning of Control Loops for Grid-Connected Modular Multilevel Converters under a Simplified Port Representation for Large System Studies

Santiago Sanchez, Gilbert Bergna, Elisabetta Tedeschi  
Norwegian University of Science and Technology  
Hogskoleringen 1, 7491,  
Trondheim, Norway

Email: {santiago.sanchez, gilbert.bergna, elisabetta.tedeschi}@ntnu.no

April 24, 2017

## Abstract

One of the present barriers to the widespread use of Modular Multilevel Converters (MMC) is the complexity of its control with respect to its predecessors. This paper presents a simple procedure to tune the current and energy control loops of the MMC, based on standard PI controllers and resembles control tuning approaches commonly used for 2-Level Voltage Source Converters (2L-VSC). The control design is based on a recently proposed simplified model of the MMC which is able to accurately represent the interface variables dynamics on the ac- and dc-side, which are considered as the main variables of concern from a macroscopic point of view. Furthermore, the tuning methodology guarantees the stable behaviour and correct tracking of the states. The paper presents simulation results of a typical case under the proposed tuning procedure.

## 1 Introduction

High-Voltage Direct-Current (HVDC) links are an attractive solution for integrating offshore wind power located far from the shore [6]. This is particularly the case in the North Sea, where the long distances between the offshore wind power generation and the onshore loads make the HVDC interconnection the preferred choice over the HVAC one. Furthermore, HVDC networks will be more and more based on Voltage Source Converter (VSC) technology, due to the possibility of reversing the power flow without voltage polarity reversal and independent controllability of active and reactive powers. In this context, the Modular Multilevel Converter (MMC) depicted in Fig. 1 is establishing itself as the most suitable converter topology due to its improved harmonic ac-voltage output, avoiding the need of installing harmonic filters [1], its lower losses and scalability associated to its modular structure [11].

The increased complexity of its control related to its additional internal energy and current dynamics has been considered a disadvantage compared to the well established 2L-VSC. This paper aims to contribute to decrease the inherent complexity of the MMC control design. This is done by presenting a simplified tuning strategy based on modulus and symmetrical optimum techniques [2], which can significantly ease the design of the control loops. Moreover, an additional inner loop tuning method is considered for regulating the converter currents based on the pole placement technique and is compared with the modulus optimum.

For both of the tuning strategies, a simplified model of the MMC suited for large-power-system oriented studies is being considered, where only the interface variables at the dc- and ac- side are taken into account in addition to the governing power balance associated to the converter distributed energy storage, following what has been presented in [5, 9, 12].

The paper is organized as follows. Section 2 describes the MMC model used and the controllers modulus optimum plus symmetrical optimum, and pole placement plus symmetrical optimum. The point-to-point HVDC topology is addressed in section 3. The results are presented in 4. Finally, the conclusions are in section 5.

## 2 MMC model and controller design

The dynamics of the simplified MMC depicted on the right hand side of Fig. 1 are represented in the synchronous reference frame by the set of equations (1)-(3), where  $\mathbf{i} = i_d + j \cdot i_q$  is the ac current in the synchronous reference frame,  $\mathbf{E} = E_d + j \cdot E_q$  is the voltage driving the ac-grid current of the MMC, while  $\mathbf{v} = v_d + j \cdot v_q$  is the voltage at the point of common coupling.

$$L \frac{d\mathbf{i}}{dt} = \mathbf{E} - \mathbf{v} - R\mathbf{i} - j \cdot \omega L \mathbf{i} \quad (1)$$

$$L_{dc} \frac{di_{dc}}{dt} = -R_{dc}i_{dc} + v_{dc} - 2u_{cz} \quad (2)$$

$$\frac{dW_z}{dt} = \left( 2u_{cz} \frac{i_{dc}}{3} - \frac{1}{2} \Re(\mathbf{E}^* \mathbf{i}) \right) \quad (3)$$

Moreover, the ac equivalent inductance and resistance are defined as  $L = L_f + L_a/2$  and  $R = R_f + R_a/2$ , respectively; where  $L_f$  and  $R_f$  are respectively the ac output filter equivalent inductance and resistance, and  $L_a$  and  $R_a$  are the equivalent inductance and resistance of the MMC arm inductor. The zero sequence energy  $W_z$  is derived from the addition of the energy of the aggregated sub-module voltages (i.e. the voltage at the upper and lower arms). After this mathematical operation the energy equations in  $abc$  are added and divided by 3, following the procedure shown in [5, 9]. This variable can be used to accurately represent the power balance between the dc and ac interfaces of the converter in a simplified way. In addition,  $i_{dc}$  represents the dc current flowing into the converter dc terminals, and can sometimes be expressed as a third of the zero-sequence circulating current  $i_{cz}$ . An equivalent MMC dc-side inductance and resistance can be conveniently defined as  $L_{dc} = (2/3)L_a$  and  $R_{dc} = (2/3)R_a$ , respectively. Finally,  $u_{cz}$  is the zero sequence voltage driving the zero-sequence circulating current  $i_{cz}$ . The reader is referred to [5] for the full details of the modelling approach.

From [5] and (1)-(3), it is possible to derive the pu simplified MMC system defined by the equations (4)-(6),

$$\frac{L_{pu}}{\omega_b} \frac{d\mathbf{i}_{pu}}{dt} = \mathbf{E}_{pu} - \mathbf{v}_{pu} - j\omega_{pu}L_{pu}\mathbf{i}_{pu} - R_{pu}\mathbf{i}_{pu} \quad (4)$$

$$\frac{L_{dcpu}}{\omega_b} \frac{di_{dcpu}}{dt} = -R_{dcpu}i_{dcpu} + v_{dcpu} - 2u_{czpu} \quad (5)$$

$$\frac{dW_{zpu}}{dt} = \frac{\omega_b}{8C_{eqpu}} (2u_{czpu}i_{dcpu} - \Re\{\mathbf{E}_{pu}^* \mathbf{i}_{pu}\}) \quad (6)$$

where the base value for the apparent power is  $S_b = 3v_b/2i_b$ . The base frequency is  $f_b$  and base electrical speed  $\omega_b = 2\pi f_b$ , the base impedance is defined as  $Z_b = v_b/i_b$ , the base inductor is  $L_b = Z_b/\omega_b$ , the base capacitor is  $C_b = 1/(Z_b\omega_b)$ . At the dc side the following base system is used; the dc power base is  $P_{dcb} = S_b$ , with the dc base voltage as  $v_{dcb} = 2v_b$ , the dc base current is  $i_{dcb} = \frac{3}{4}i_b$ , the base impedance is defined as  $Z_{dcb} = v_{dcb}/i_{dcb}$ , using the dc base inductor  $L_{dcb} = Z_{dcb}/\omega_b$  and the base dc capacitor is  $C_{dcb} = 1/(Z_{dcb}\omega_b)$ . The energy base of the system can be calculated as  $W_b = S_b/\omega_b$ . Finally, the single phase reference energy is  $W_{ref} = 2 * n_{arms}C_{eq}V_b^2$ , where  $n_{arms}$  is the number of arm per leg of the MMC.

### 2.1 Controller design

The simplified MMC is controlled with multiple loops in a cascaded structure, as shown in Fig. 2. First, the reference of the active component of the ac grid current  $i_d^*$  is calculated by an outer loop controller to regulate the energy  $W_z$  to its reference value  $W_z^*$ . In addition, the reference of the reactive component of the ac current  $i_q^*$  is set to zero. Both the active and reactive components of the ac current are regulated to follow their respective references by means of an inner loop controller. The second part uses a single current control loop to regulate the current  $i_{cz}$  to a desired reference  $i_{cz}^*$ , which imposes the power transfer of the converter.

The basic controller used for the MMC in this paper is the PI controller given its success in the power electronic industry [10], and it will be shown how it can be applied both to the current and energy controllers of the MMC. The standard model used in the PI based control of power electronics is shown in Fig. 3, where  $Y_{ref}$  is the reference value,  $Y$  is the output of the system,  $U$  is the controller output,  $D$  is a disturbance term, and  $K_p$  and

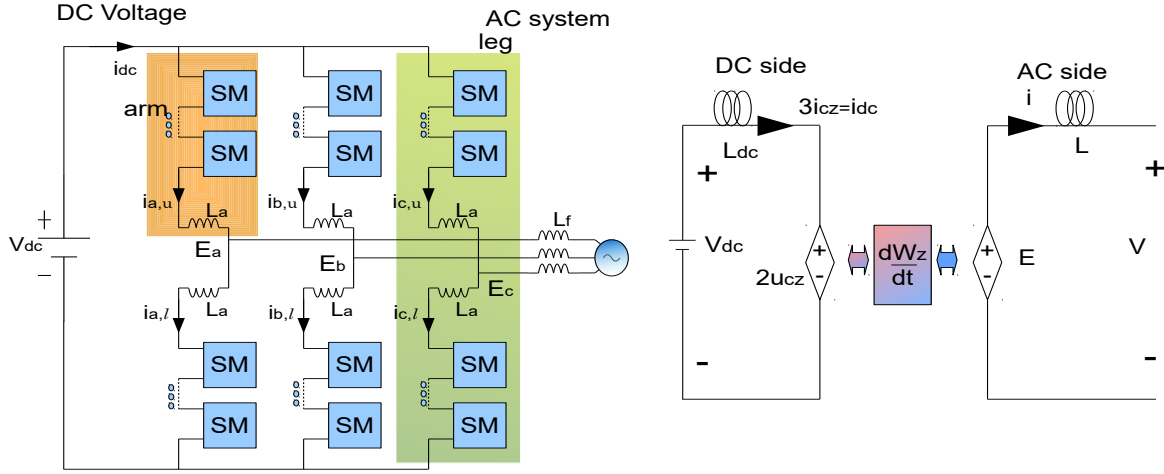


Figure 1: Complete model (left) and Energy based simplified model (right) of the MMC.

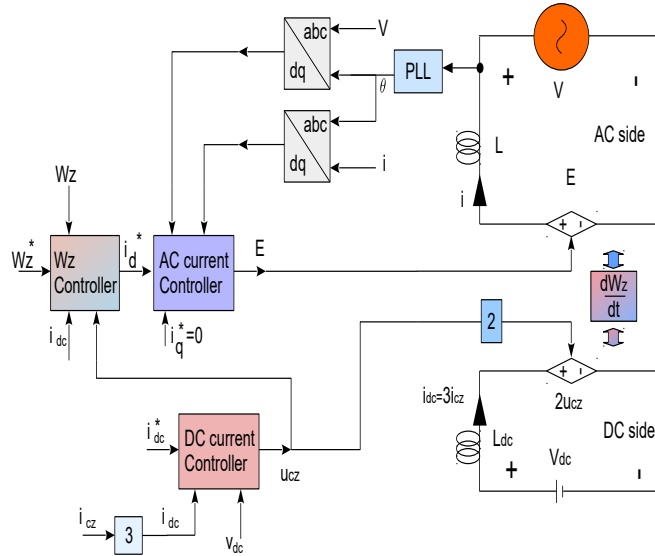


Figure 2: Block diagram control strategy of the simplified MMC.

$K_i$  are the proportional and integral gains, respectively. For the block representation, the PI controller can be shown in the Laplace domain as:

$$U = (K_p + \frac{K_i}{s})(Y_{ref} - Y) - D. \quad (7)$$

## 2.2 Modulus optimum and lead compensator

The system to be controlled by the current regulators takes the general form shown in (8) [2],

$$H(s) = \frac{k}{(1 + sT)(1 + sT_f)}, \quad (8)$$

where  $H(s)$  is a general second order transfer function and is used to represent the current dynamics for the ac and dc side with the dynamics of the switches and measurement filters of the MMC converter. The time constant  $T_f$  represents the dynamics of the filters and modulation in the converter,  $T$  represents the dominant pole of the system, while  $k$  is a generic constant. The poles of the system are real and it can be assumed that  $T \gg T_f$ .

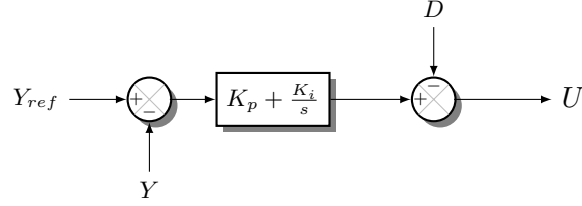


Figure 3: Block diagram in the Laplace domain for standard control in power electronics.

For the ac current side system  $k = 1/R_{pu}$  and  $T = L_{pu}/(\omega_b R_{pu})$ . Furthermore, the dc side current loop uses  $k = 1/R_{dcpu}$  and  $T = L_{dcpu}/(\omega_b R_{dc})$ .

The use of modulus optimum from [2] gives a proportional plus integral controller structure for the system in (8). Therefore, the controller is  $G_c(s) = K_p + K_p/(sT_i) = K_p + K_i/s$ . According to this strategy, the final values of the controller are:

$$K_p = \frac{T}{2T_f k}, \quad T_i = T, \quad K_i = K_p/T_i. \quad (9)$$

Finally, the closed loop transfer function of the inner system is:

$$H_{cl}(s) = \frac{0.5}{T_f^2 s^2 + T_f s + 0.5} \quad (10)$$

The second order system in (10) can be approximated by a first order system of the form  $H_{ap}(s) = 1/(T_{eq}s + 1)$  (see Fig. 4). Taking  $T_{eq} = 2T_f$ , then a control strategy as the lead compensator, also known as 'symmetrical optimum', can be applied to the outer system which represents the energy  $W_z$ . The lead compensator in [7] is designed for the systems with open loop transfer function as in (11).

$$H_{olout}(s) = K_p \frac{(s+z)}{s} \frac{1}{s+p} \frac{b}{s}, \quad (11)$$

where  $W_{zpu}$  in (6) has the form of an integrator model in Laplace domain. This system has transfer function  $H_p(s) = b/s$ , which represents the energy  $W_{zpu}$  model with  $b = \omega_b/(8C_{eqpu})$ . The internal current loop used to balance the power is the ac current system (i.e. the output of the energy controller is the reference current for the direct axis). The controller can be written as  $G_c(s) = K_p \frac{s+z}{s}$  and is in the form of a PI controller. Moreover, the equivalent inner system is  $H_{ap}(s) = \frac{1}{p+s}$ , with  $p = 1/T_{eq}$  (see Fig. 4). Finally,  $z$  is chosen as  $z = p/\alpha$  where the gain  $\alpha$  is an input from the designer that complies with  $\alpha > 1$ . The controller is designed with the set of equations:

$$\omega_m = \sqrt{zp}, \quad K_p = \frac{\omega_m}{b}, \quad (12)$$

where,  $\omega_m$  is the geometric mean of the zero and pole, while the phase margin  $\phi_m$  is the maximum phase angle achieved, which is in turn dependent on the selected  $\alpha$ . It can be calculated using  $\sin(\phi_m) = \frac{\alpha-1}{\alpha+1}$ . In this work  $\alpha = 6$  is used, corresponding to a phase angle of  $\phi_m = 45.58$  degrees.

### 2.3 Pole placement and lead compensator

The direct, quadrature and dc current systems can be represented in a general form as in (13), which is the equivalent transfer function of the voltage across the series resistor and inductor. It can be seen as an approximation of (8) using the dominant pole  $T$ .

$$H_{dom}(s) = \frac{c}{s+a} \quad (13)$$

In (13),  $c = \omega_b/L_{kpu}$  is a parameter depending on the inductance used in equations (4) and (5) (i.e. the inductor  $L_{kpu}$  is  $L_{pu}$  for the ac side or  $L_{dcpu}$  for the dc side and used for each PI controller tuning) [2, 10]. In addition,

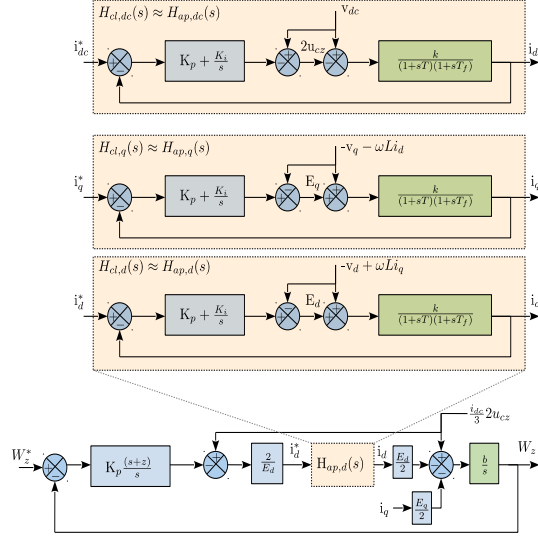


Figure 4: Closed loop systems and their use on the control strategy.

the parameter  $a = \omega_b R_{kpu} / L_{kpu}$  depends on the inductance and resistance of each terminal of the converter. In order to obtain the controller parameters, the standard second order characteristic polynomial equation (14) is used.

$$A(s) = s^2 + 2\rho\omega_o s + \omega_o^2 \quad (14)$$

where  $\omega_o$  determines the response speed and  $\rho$  is the damping ratio which determines the shape of the response. The characteristic polynomial of the closed loop controlled system is  $s^2 + (cK_p + a)s + cK_i$ . Moreover, identifying the coefficients of (14) and the closed loop of the controlled system, the controller gains in (15) and (16) are obtained.

$$K_p = \frac{2\rho\omega_o - a}{c} \quad (15)$$

$$K_i = \frac{\omega_o^2}{c} \quad (16)$$

In order to obtain a good damped response, the damping parameter is set to  $\rho = 1.1$  and the natural frequency to  $\omega_o = \beta a$ , with a gain  $\beta > 1$ . The tuning of the controllers by pole placement in this paper uses  $\beta = 5$ .

The outer loop (i.e. the energy controller) uses the lead compensator described in the previous subsection. In this closed loop the equivalent time constant is evaluated as  $T_{eq} = 2/(\rho\omega_o)$ .

### 3 Case study: point-to-point HVDC link

The MMC-HVDC topology used for the test of the controllers is presented in Fig. 5. It is based on the recommendations of the CIGRE guide for HVDC grids [3]. For this test a monopole configuration is employed. The currents  $i_{dck}$  are the current at terminals of the simplified MMC as defined in section 2,  $i_{lok}$  is the current going in the station and  $k$  is used for the  $k$ -th node of the point-to-point link. Furthermore,  $C_{pk}$  is the pole capacitor at each node. Each simplified MMC converter has the structure described in Fig. 1. In addition, the cable model uses the structure defined in [4] and takes the frequency variation of the parameters into account. This parametric frequency dependence is represented by means of multiple parallel RL-branches as shown in Fig. 5, where  $R_{lm}$  and  $L_{lm}$  are the series resistor and inductor per branch respectively, with  $m \in \{1, 2, 3\}$ . Finally,  $C_l$  and  $G_l$  are the capacitor and conductance of the line, respectively.

The power equation of the dc link at each node is described in (17) based on the energy stored in  $C_{dck}$ . The input power is  $P_{lok} = v_{dck} i_{lok}$ , while the converter power at the dc link is  $P_{dck} = v_{dck} i_{dck}$ . Equation (18) presents the per unit system. The controller configuration has been applied as recommended in [10].

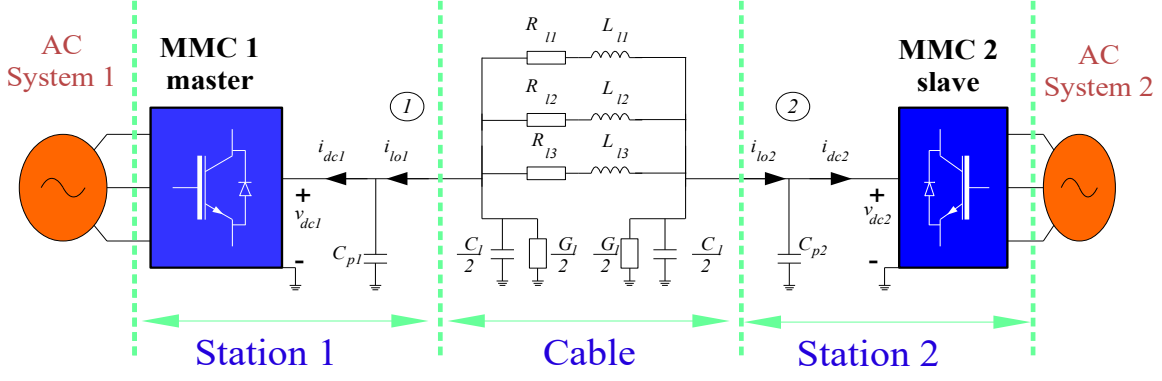


Figure 5: Point-to-point link.

Table 1: Parameters of the MMC simplified model.

Parameter	value
$R_a$	0.6017 [ $\Omega$ ]
$L_a$	30.6000 [mH]
$R_f$	0.6438 [ $\Omega$ ]
$L_f$	78.2000 [mH]
$C_p$	150 [ $\mu$ F]
$C_{eq}$	21.1600 [ $\mu$ F]

$$\frac{1}{2}C_{dck} \frac{dv_{dck}^2}{dt} = P_{lok} - P_{dck} \quad (17)$$

$$\frac{C_{dcpuk}}{2\omega_b} \frac{dv_{dcpuk}^2}{dt} = P_{lopuk} - P_{dcpuk} \quad (18)$$

Using the solution from [10] to control  $v_{dck}$  in (18), the power reference  $P_{dcpuk}^*$  sent to the converter is shown in the Laplace domain in (19). The PI controller is designed with the method used in subsection 2.2. The system uses feed-forward of the input power through a low-pass filter  $H_{dc}(s)$ .

$$P_{dcpuk}^* = H_{dc}(s)P_{lopuk} - \left( K_p \frac{s+z}{s} \right) (v_{dcpuk}^2 * -v_{dcpuk}^2) \quad (19)$$

The controller parameters can be found using the lead compensator design described in subsection 2.2. In this case the parameter  $b = (2\omega_b)/C_{dcpuk}$  and  $p$  are selected based on the controller used in the dc current inner loop. In case the modulus optimum is applied, then  $T_{eq} = 2T_f$ . When the pole placement dc current controller is applied, then  $T_{eq} = 2/(\rho\omega_o)$  as described in subsection 2.3.

## 4 Simulation results

The application of the proposed tuning techniques to both MMCs used on the HVDC link of Fig. 5 is analysed. The goal is to use MMC 1 in a master configuration, by controlling the voltage between its dc terminals. By contrast, MMC 2 is controlled in a slave configuration, where it regulates the power consumed by the systems by means of the dc current regulation. The energy  $W_z$  is regulated at the same time around a set point in both converters. The base apparent power is  $S_b = 1200$  MVA and the base voltage is  $V_b = 400$  kV. Table 1 presents the parameters of the MMC. The switching signals and measurement filters for this type of system are in the range [0.5 – 10] kHz. A cut-off frequency of  $f_{co} = 2$  kHz has been selected, implying  $T_f = 1/(2\pi f_{co})$ . The approximations on the ac system used for the procedures above are compared with the normal models of (8) and the resulting closed loop transfer function of each procedure. The approximations for the case of modulus

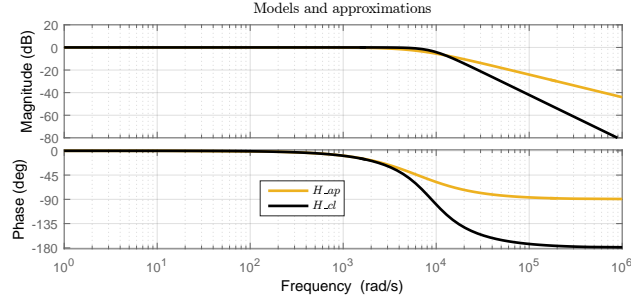


Figure 6: Approximations of the models used in the design of the modulus optimum and lead compensator.

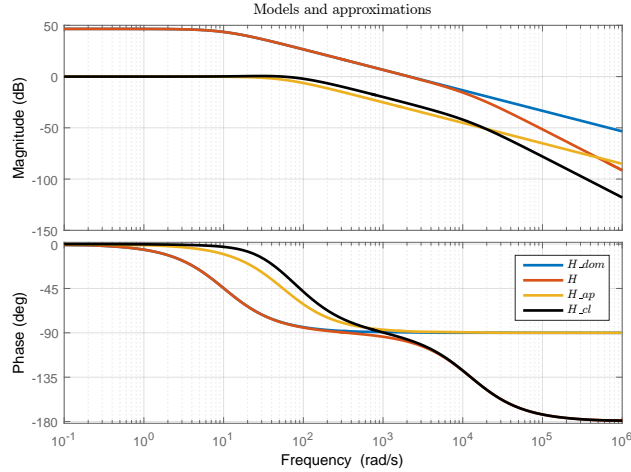


Figure 7: Approximations of the models used in the design of the pole placement and lead compensator.

optimum and lead compensator are shown in Fig. 6. Initially, the closed loop  $H_{cl}$  in (10) (black curve) is compared with the approximated model  $H_{ap}$  (yellow curve). It is shown that they are close below the  $10^3$  rad/s, and that  $H_{ap}$  has cut-off frequency  $1/(2T_f)$ .

The approximations for the case of pole placement and lead compensator are shown in Fig. 7. First, the approximation of the close loop current controller with pole placement used in subsection 2.3 is  $H_{ap}$ . The second comparison is with the approximation in subsection 2.3 between (8) and (13). It is shown in both cases that the frequency responses are very close at low frequencies (i.e. for large magnitudes), and they differ when the frequency is around  $10^4$  rad/s.

Figure 8 and Fig. 9 show the closed loop frequency response of the inner and outer loop. The bandwidth for the controllers is shown as well. The current controller presents a faster dynamic than the external loop ( $H_{clW_z}$  and  $H_{clv_{dc}}$ ). The dc current closed loop presents a similar behaviour than the ac current closed loop.

#### 4.1 Point-to-point link with modulus optimum and lead compensator

In this subsection the controllers parameters are calculated with the modulus optimum for the current controllers and the lead compensator for the energy  $W_z$  controller in both converters. The voltage is controlled by the master converter and the parameters of the controller are calculated with the lead compensator. The time response of the system is shown in Fig. 10 and Fig. 11. The selected transient shows the behaviour of the currents and the tracking of the references. Moreover, the signals overlap during the transient shown. The simulation presents two step changes in the current at the dc side to represent the power injection with the MMC 2 (slave). In Fig. 11 the successful regulation of  $W_z$  and  $v_{dc}$  is shown, where the MMC 1 is in charge of the regulation of the voltage at the node 1. The controller of  $W_z$  in each converter sends the current reference for the ac inner controllers (Fig. 10). Therefore, the power is balanced between the ac and dc sides in each converter.

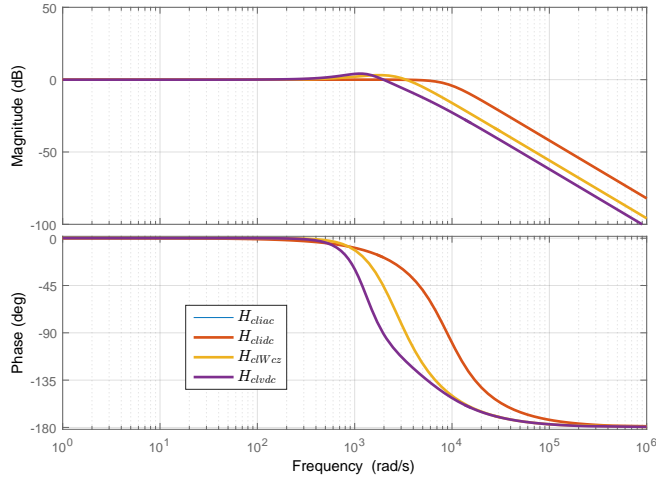


Figure 8: Energy, dc voltage and current closed loop frequency response with modulus optimum and lead compensator.

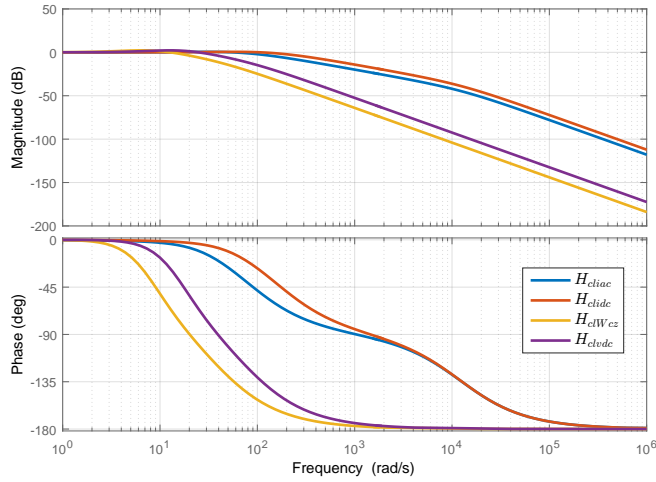


Figure 9: Energy, dc voltage and current closed loop frequency response with pole placement and lead compensator.

## 4.2 Point-to-point link with pole placement and lead compensator

The final test applies the pole placement technique on the current controllers and the lead compensator as described in subsection 4.1. The time response of the system is shown in Fig. 12 and Fig. 13. Moreover, the test is as described before with two time steps in the power injected by the slave MMC at node 2. In this case an overshoot can be observed from the regulation of  $W_z$  and  $v_{dc}$  (Fig. 13). This overshoot can be reduced by increasing  $\beta$ , which makes faster the internal current controllers.

## 5 Conclusion

Two simple techniques to tune the controller parameters in a PI-based cascaded structure have been evaluated on a simplified MMC model that accurately captures the dynamical behaviour between its dc and ac terminals. The implemented tuning strategies are based on the natural time constants of the currents in the ac and dc side circuits of the simplified MMC model, as well as on the power balance equation represented by the aggregated capacitive energy dynamics of the converter. In general, the modulus optimum controller includes the dynamics of the different digital filters and measurement equipment. By contrast, the pole placement uses the time constant of the passive filter elements of the MMC.

The two different control tuning techniques were presented on a case scenario consisting on a point-to-point

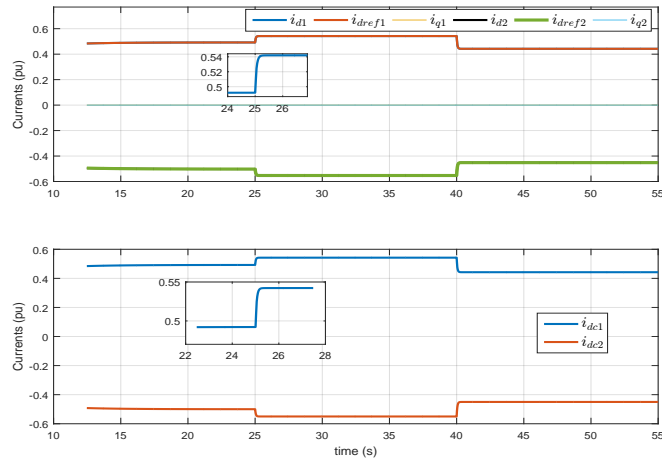


Figure 10: AC and dc currents time response for each MMC in the point-to-point link.

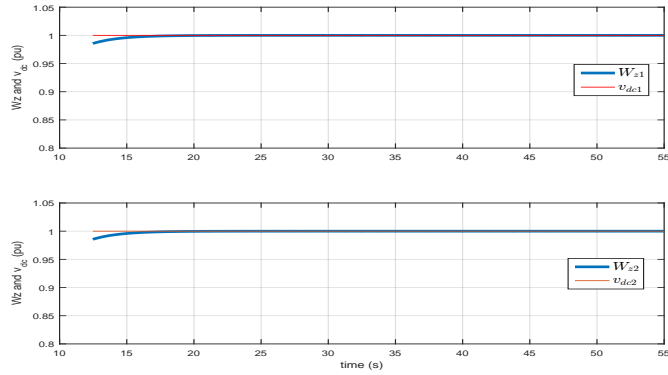


Figure 11: Energy  $W_z$  and dc voltage  $v_{dc}$  time response for each MMC in the point-to-point link.

HVDC system interconnected by a cable model able to capture the frequency dependence of the parameters. It is possible to get better performance of the current control with the pole placement method by increasing the  $\beta$  tuning parameter. It is important to highlight that during the design stage of the controller, the choice of the technique can be based on the available information of the system. For instance, a designer without information about the filter could not tune the controller using the modulus optimum. Hence, this designer can apply the pole placement strategy.

The second-order to first-order transfer function approximations that have been used in the tuning procedure has been validated with a comparison of the frequency responses, as discussed in the simulation result section.

## 6 Acknowledgement

This project has received funding in the framework of the joint programming initiative ERA-Net Smart Grids Plus, with support from the European Union's Horizon 2020 research and innovation programme and Research council of Norway.

## Appendix

### 6.1 Parameters of the dc cable

The cable model in the point-to-point link is based on [8], the parameters are listed in Table 2.

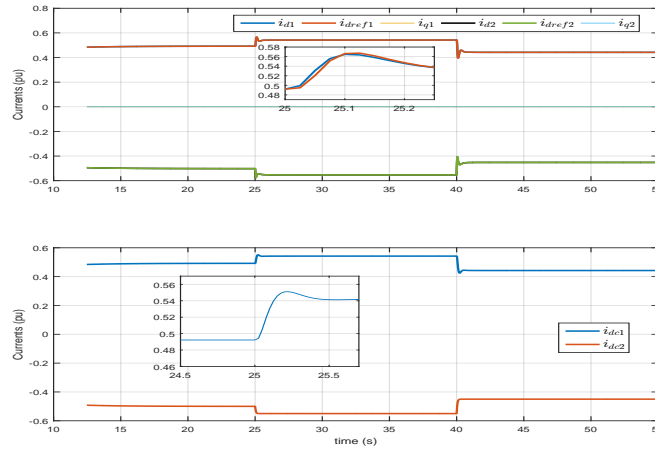


Figure 12: AC and dc currents time response for each MMC in the point-to-point link.

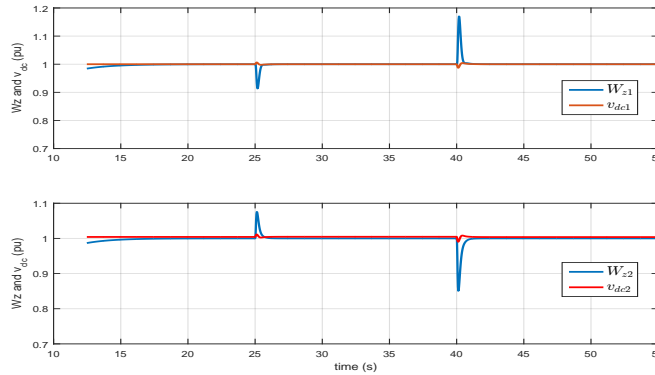


Figure 13: Energy  $W_z$  and dc voltage  $v_{dc}$  time response for each MMC in the point-to-point link.

## References

- [1] R. Adapa. High-wire act: Hvdc technology: The state of the art. in *IEEE Power and Energy Magazine*, 10(6):18–29, 2012.
- [2] Karl Johan Åström and Tore Hägglund. *Advanced PID Control*. ISA - The Instrumentation, Systems, and Automation Society, Research Triangle Park, NC 27709, 2005.
- [3] Working Group B4.57. *Guide for the Development of Models for the HVDC Converters in a HVDC Grid*. CIGRE, 2014.
- [4] J. Beerten, J.A. Suul, and S. D’Arco. Cable model order reduction for hvdc systems interoperability analysis. In *11th IET International Conference on AC and DC Power Transmission*, pages 1–10, Feb 2015.

Parameter	value	Parameter	value
$R_{11}$	$1.1724 \cdot 10^{-1}$ [ $\Omega/\text{km}$ ]	$L_{11}$	$2.2851 \cdot 10^{-4}$ [H/km]
$R_{12}$	$8.2072 \cdot 10^{-2}$ [ $\Omega/\text{km}$ ]	$L_{12}$	$1.5522 \cdot 10^{-3}$ [H/km]
$R_{13}$	$1.1946 \cdot 10^{-2}$ [ $\Omega/\text{km}$ ]	$L_{13}$	$3.2942 \cdot 10^{-3}$ [H/km]
$G_l$	$7.6330 \cdot 10^{-11}$ [S/km]	$C_l$	$0.1983 \cdot 10^{-6}$ [F/km]

- [5] G. Bergna-Diaz, J. A. Suul, and S. D'Arco. Small-signal state-space modeling of modular multilevel converters for system stability analysis. In *2015 IEEE Energy Conversion Congress and Exposition (ECCE)*, pages 5822–5829, Sept 2015.
- [6] M. K. Bucher and et al. Multiterminal hvdc networks—what is the preferred topology? in *IEEE Transactions on Power Delivery*, 29(1), 2014.
- [7] R.-C. Dorf and R.-H. Bishop. *Modern Control Systems*. Addison Wesley, 7th edition, 1995.
- [8] J. Freytes, S. Akkari, J. Dai, F. Gruson, P. Rault, and X. Guillaud. Small-signal state-space modeling of an hvdc link with modular multilevel converters. In *2016 IEEE 17th Workshop on Control and Modeling for Power Electronics (COMPEL)*, pages 1–8, June 2016.
- [9] J. Freytes, L. Papangelis, H. Saad, P. Rault, T. Van Cutsem, and X. Guillaud. On the modeling of mmc for use in large scale dynamic simulations. In *2016 Power Systems Computation Conference (PSCC)*, pages 1–7, June 2016.
- [10] L. Harnefors, M. Bongiorno, and S. Lundberg. Input-admittance calculation and shaping for controlled voltage-source converters. *Industrial Electronics, IEEE Transactions on*, 54(6):3323 –3334, dec. 2007.
- [11] A. Lesnicar and R. Marquardt. An innovative modular multilevel converter topology suitable for a wide power range. In *Power Tech Conference Proceedings, 2003 IEEE Bologna*, volume 3, pages 6 pp. Vol.3–, June 2003.
- [12] D. C. Ludois and G. Venkataramanan. Simplified terminal behavioral model for a modular multilevel converter. *IEEE Transactions on Power Electronics*, 29(4):1622–1631, April 2014.